Available online at www.sciencedirect.com

SCIENCE DIRECT®

Journal of Controlled Release 105 (2005) 185–198

journal of controlled release

www.elsevier.com/locate/jconrel

Influence of administration route on tumor uptake and biodistribution of etoposide loaded solid lipid nanoparticles in Dalton's lymphoma tumor bearing mice

L. Harivardhan Reddy[a], R.K. Sharma[b], K. Chuttani[b], A.K. Mishra[b], R.S.R. Murthy[a,*]

[a]*Drug Delivery Research Laboratory, Center of Relevance and Excellence in NDDS, Pharmacy Department, G.H. Patel Building, Donor's Plaza, M.S. University, Fatehgunj, Baroda-390002, Gujarat, India*

[b]*Division of Radiopharmaceuticals and Radiation Biology, Institute of Nuclear Medicine and Allied Sciences, Brig. S.K. Mazumdar Road, Delhi-110 054, India*

Received 26 April 2004; accepted 21 February 2005
Available online 24 May 2005

Abstract

The study evaluates the capability of tripalmitin nanoparticles in enhancing the tumor uptake of etoposide, and the influence of administration route on the biodistribution and tumor uptake of etoposide loaded tripalmitin (ETPL) nanoparticles in Dalton's lymphoma tumor bearing mice. ETPL nanoparticles were prepared by melt-emulsification and high pressure homogenization followed by the spray drying of nanodispersion. Characterization of the nanoparticles was done by particle size analysis, zeta potential measurement and scanning electron microscopy. The size of ETPL nanoparticles was 387 nm and possessed negative charge. Etoposide and ETPL nanoparticles were radiolabeled with ^{99m}Tc with high labeling efficiency. The labeled complexes showed good in vitro stability in the presence of DTPA/cysteine and serum stability. Etoposide and ETPL nanoparticles were injected by subcutaneous, intravenous or intraperitoneal routes and their biodistribution and tumor uptake were determined. Subcutaneous injection reduced the distribution of ETPL nanoparticles to all the tissues studied whereas after intraperitoneal injection, the distribution of ETPL nanoparticles to tissues was higher than free etoposide. The intravenous injection resulted in lower concentrations of ETPL nanoparticles in the organs of RES compared to free etoposide. ETPL nanoparticles experienced significantly high brain distribution after intraperitoneal injection indicating its potential use in targeting etoposide to brain tumors. After subcutaneous injection, the tissue distribution of ETPL nanoparticles increased with time indicating their accumulation at the injection site for a longer time. The tumor uptake of both etoposide and ETPL nanoparticles was significantly high after subcutaneous injection ($P<0.001$) compared to the other routes of administration. The tumor concentration of ETPL nanoparticles after subcutaneous injection was 59 folds higher than that obtained after intravenous and 8 folds higher than after intraperitoneal route at 24 h post-injection. The tumor concentration of ETPL nanoparticles increased with time after subcutaneous injection indicating the slower and progressive penetration from the injection site into the tumor. The study signifies the advantage of incorporating etoposide into tripalmitin nanoparticles in controlling its biodistribution and enhancing the tumor uptake by several folds. The study also reveals that, of the three routes investigated,

* Corresponding author. Tel.: +91 265 2794051; fax: +91 265 2423898.
E-mail address: m_rsr@rediffmail.com (R.S.R. Murthy).

0168-3659/$ - see front matter
doi:10.1016/j.jconrel.2005.02.028

subcutaneous injection is the route of preference for facilitating high tumor uptake and retention and is likely to have greater antitumor effect resulting in tumor regression.

Keywords: Etoposide; Technetium-99 m; Solid lipid nanoparticles; SLN; Subcutaneous injection; Dalton's lymphoma tumor

1. Introduction

Drug targeting and transport to solid tumors have been the area of extensive focus in the field of drug delivery. Despite several advancements, the drug transport at high concentrations to solid tumors seems still to be a challenge. Recently, several drug modifications [1], carrier systems [2–5] and techniques such as ultrasound [6] were attempted to improve the tumor reach of anticancer agents. Nanoparticles have been widely attempted for delivering anticancer agents to tumors [7–9]. Great attention was observed in the use of lipid nanoparticles as drug carriers because they combine the advantages of polymeric nanoparticles, fat emulsions and liposomes while simultaneously overcoming their drawbacks [8–11]. The in vitro cytotoxicity studies have proved that the lipid nanoparticles cause low toxicity relative to polymeric nanoparticles [12,13]. Not many reports are available on the use of lipid nanoparticles as drug carriers for the targeted delivery of anticancer agents to tumors.

Different routes of administration may result in varying effects on the biodistribution pattern of drug carriers. Allen and coworkers [14] have compared the biodistribution pattern of liposomes administered through different routes and reported wide differences in the tissue distribution of liposomes. Thus, the route of administration appears to be an important parameter in the delivery of anticancer agents to tumors.

Dalton's lymphoma is a T-cell lymphoma and is grown in the hind leg of mice after subcutaneous implantation of tumor cells. According to Muranishi and coworkers [15] and Takahashi [16], tumor cells that have invaded a lymphatic vessel would be trapped in the meshwork of a lymph node. Hence, the approaches taken to enhance the tumor delivery to Dalton's lymphoma should match with that of approaches suggested for improvement of lymph node targeting. For effective penetration into lymphatic interstitium, the carrier systems are required to possess smaller size, hydrophobicity and negative surface charge [17]. The lipid nanoparticles proposed by us possess all the above characteristics, and are attempted to enhance the delivery of etoposide to Dalton's lymphoma tumor. Etoposide inhibits topoisomerase II and has been used in the treatment of a variety of malignancies like malignant lymphoma, brain stem gliomas, SCLC (small cell lung carcinoma), stomach cancer and ovarian cancer. Inhibition of topoisomerase II and activation of oxidation reduction reactions induced by etoposide to produce derivatives that binds directly to DNA cause DNA damage [18,19].

For improved lymphatic transport of drug carriers, the subcutaneous [20] and intraperitoneal routes have been suggested earlier [21]. The smaller size of the drug carriers is also reported to facilitate the infiltration into tumor interstitium through the leaky tumor vasculature [22]. However, this needs to be investigated in case of lipid nanoparticles. Hence to get an insight into the in vivo behavior of lipid nanoparticles and identify the superior route contributing to major tumor uptake, their biodistribution was studied after different routes such as intravenous, intraperitoneal and subcutaneous injection.

The aim of the present study is to evaluate the capability of tripalmitin nanoparticles to enhance the tumor uptake of etoposide, and investigate the influence of administration route on the biodistribution and tumor uptake of etoposide and etoposide loaded tripalmitin (ETPL) nanoparticles in mice bearing Dalton's lymphoma tumor. ETPL nanoparticles were prepared by melt-emulsification and high pressure homogenization followed by the spray drying of nanodispersion. Characterization of the nanoparticles was done by particle size determination, zeta potential measurement and scanning electron microscopy. Etoposide and ETPL nanoparticles were administered by subcutaneous, intravenous or intraperitoneal routes and their biodistribution, tumor uptake and retention were determined.

2. Materials and methods

2.1. Chemicals

Etoposide was a gift sample obtained from Dabur Research Center (India) and Cipla Limited (India). Tripalmitin was purchased from Sisco laboratories (India). Hydrogenated Soya Phosphatidyl Choline (HSPC) was purchased from Lipoid (GMBH). Diethylene triamine penta acetic acid (DTPA) and Cysteine were purchased from Sigma Chemical Co., USA. Sodium tauroglycocholate and stannous chloride were purchased from Qualigens (India). Sodium pertechnetate eluted from molybdenum-99 by solvent extraction, was procured from the Regional Center for Radiopharmaceutical Division (Northern Region), Board of Radiation and Isotope Technology (BRIT), Delhi, India. All other chemicals used in the study were of analytical reagent grade.

2.2. Preparation of etoposide loaded tripalmitin nanoparticles

ETPL nanoparticles were prepared by melt emulsification and homogenization technique. Briefly, the etoposide was dissolved in hydrogenated soya phosphatidyl choline (HSPC) (drug–lipid ratio of 1:29) and to it was added tripalmitin (tripalmitin–HSPC ratio of 4:1) and melted by heating up to 85 °C. The hot melt was emulsified using a blade-type stirrer (Remi, Mumbai, India) at 2000 rpm into the aqueous phase containing 3% w/v sodium tauroglycocholate which was pre-heated to 5 °C above the temperature of the lipid phase, and the stirring was continued for 2 min. The hot emulsion was then homogenized at a pressure of 10,000 psi for 3 cycles in the high pressure homogenizer (Emulsiflex C5, Avestin, Ottawa, ON, Canada) maintained in water bath at 90 °C. The nanodispersion formed was spray dried after the addition of 2 parts by weight lactose monohydrate.

2.3. Determination of drug content in ETPL nanoparticles

The nanoparticles in dispersion were aggregated by adding 0.1 ml of 10 mg/ml protamine sulphate solution and centrifuged the dispersion at 3000 rpm for 5 min to obtain the pellet. The supernatant was decanted and pellet was washed with distilled water and lyophilized after the addition of 2 parts by weight sucrose with respect to total lipid content of the formulation. Twenty-five milligrams of lyophilized powder was dissolved in a mixture of Methanol–Chloroform (1:1), required dilutions were performed with the same solvent mixture and analyzed in UV-Visible spectrophotometer at 286 nm against the solvent blank containing same concentration of HSPC used in the nanoparticles.

2.4. Characterization of tripalmitin nanoparticles

2.4.1. Particle size analysis

The size analysis of ETPL nanoparticles was performed by dynamic light scattering using Malvern Hydro 2000SM particle size analyzer (Malvern Instruments, UK). The dry nanoparticulate powder was dispersed into the aqueous media by simply shaking twice. The aqueous nanoparticulate dispersion was added to the sample dispersion unit containing stirrer, and stirred in order to minimize the inter particle interactions, and the laser obscuration range was maintained between 10 and 20%. The analysis was performed thrice and the average values were taken.

2.4.2. Zeta potential measurement

Zeta potential of ETPL nanoparticles was measured in Malvern Zetasizer 3000 HS_A (Malvern Instruments, UK). The nanoparticles were dispersed in phosphate-buffered saline, pH 7.4 and the zeta potential was measured.

2.4.3. Scanning Electron Microscopy (SEM)

The powder nanoparticles were stuck on to a brass stub through double adhesive tape. The stub was fixed into sample holder and placed in vacuum chamber of Jeol JSM 1560 LV scanning electron microscope and observed under low vacuum (10^{-3} Torr).

2.5. Radiolabeling of etoposide and ETPL nanoparticles

Etoposide and ETPL nanoparticles were radiolabeled with Technetium-99 m (^{99m}Tc) by reduction with stannous chloride similar to the previously reported method [23,24]. Briefly, the pertechnetate

(TcO_4^-) (2 mCi) was reduced with stannous chloride (20 μg for etoposide and 60 μg for ETPL nanoparticles) and pH was adjusted to 6.5 with 0.5 M sodium bicarbonate. To it was added etoposide (2 mg/ml) or ETPL nanoparticles (equivalent to 2 mg/ml of etoposide) and incubated at room temperature for 10 min. The quality control was performed as per the method reported earlier [25]. The labeling efficiency of etoposide and ETPL nanoparticles was determined by ascending thin layer chromatography using silica gel coated fiber sheets (Gelman Sciences Inc., Ann Arbor, MI). The instant thin layer chromatography (ITLC) strip was spotted with 2 μl of the labeled complex at 1 cm above the bottom and developed using acetone as the mobile phase. The solvent front was allowed to reach up to a height of about 8 cm from the origin. The strip was cut into two halves and the radioactivity in each half was determined by a well type gamma ray spectrometer (Type GRS23C, Electronics Corporation of India Limited, India). The free pertechnetate (R_f=0.9–1.0) migrates to the top portion of the ITLC strip, leaving the reduced/hydrolyzed ^{99m}Tc along with the labeled complex at the bottom. Incorporation of excess of stannous chloride for reduction of pertechnetate may lead to the formation of undesirable radiocolloids. The radiocolloid formation was determined in pyridine: acetic acid: water (3:5:1.5). The radio colloids remained at the bottom of the strip, while both the free pertechnetate and the labeled complex migrated with the solvent front. By subtracting the migrated activity with the solvent front using acetone from that using pyridine: acetic acid: water mixture, the net amount of ^{99m}Tc-etoposide or ^{99m}Tc-ETPL nanoparticles was calculated.

2.6. In vitro serum stability of the ^{99m}Tc labeled complexes

Stability of the ^{99m}Tc labeled complexes of etoposide and ETPL nanoparticles was determined in vitro in human serum by ascending TLC technique. The labeled complex (0.1 ml) was incubated with freshly collected human serum (0.4 ml) at 37 °C up to 24 h. The samples were withdrawn at regular intervals up to 24 h and analyzed in gamma ray spectrometer. Aliquots at different time intervals were applied on ITLCSG paper and sum in of the labeled complex.

2.7. DTPA and Cysteine challenge

In order to check the strength of binding of ^{99m}Tc with the compound, 0.5 ml of the labeled preparation was challenged against various concentrations (10, 30 and 50 mM) of DTPA and cysteine [26] and incubated for 1 h at 37 °C. The effect of DTPA on labeling efficiency was measured on ITLC-SG using acetone as the mobile phase, which allowed the separation of free pertechnetate and DTPA-complex (R_f=0.8–1.0) from the ^{99m}Tc-etoposide and ^{99m}Tc-ETPL nanoparticles which remained at the point of application (R_f=0). For cysteine, 0.1M PBS (pH 7.4) was used as the mobile phase. Free pertechnetate and cysteine complex moved with the solvent front whereas the labeled moiety remained at the base.

2.8. Tumor implantation

The Dalton's lymphoma tumor cells were maintained in the peritoneum of Balb/c mice in the ascites form by serial weekly passage. Exponentially growing cells were harvested and 5×10^6 cells per mouse were injected subcutaneously in the thigh of the right hind leg. After 8–10 days, a palpable tumor in the volume range of 0.9 ± 0.1 cm^3 was observed and used for further studies.

2.9. Biodistribution study

^{99m}Tc labeled etoposide and ETPL nanoparticles were injected by subcutaneous, intravenous or intraperitoneal routes into the tumor bearing Balb/c mice weighing about 25–30 g. The biodistribution was performed at 1 h, 6 h and 24 h post-injection. At these time intervals, the blood was collected by cardiac puncture and animals were sacrificed and the organs were isolated. The organs were then weighed and measured for radioactivity in gamma ray spectrometer. The radioactivity was interpreted as % injected dose (% ID) per gram of organ/tissue. All the animal experiments were approved by the Social Justice and Empowerment Committee for the purpose of control and supervision of experiments on animals (CPCSEA), Government of India, New Delhi.

2.10. Tumor imaging by gamma scintigraphy

One hundred μCi of the ^{99m}Tc-ETPL nanoparticle complex was injected by subcutaneous or intravenous injection below the tumor region on the right hind leg of mice bearing Dalton's lymphoma tumor. At 24 h post-injection, the mice were fixed on animal fixing tray board and imaging was performed with Single Photon Emission Computed Tomography (SPECT, LC 75-005, Diacam, Siemens, USA) gamma camera.

2.11. Statistical analysis

Statistical comparisons of the experimental results were performed by student's *t*-test at significance level of 0.01 and 0.001.

3. Results

ETPL nanoparticles were prepared by melt emulsification and high pressure homogenization technique. The powdered nanoparticles were obtained by spray drying of the nanodispersion. The technique yielded spherical powder particles (Fig. 1) with excellent redispersibility in aqueous media. The mean diameter of nanoparticles in nanodispersion form and after spray drying was determined. The mean diameter of particles was found only slightly increased after spray drying (358 nm before spray drying and 387 nm after spray drying), and the size distribution being unimodal both before and after spray drying. The nanoparticles exhibited negative zeta potential (−46.6 mV). ETPL nanoparticles were loaded with 4% etoposide with an entrapment efficiency of 98.96%.

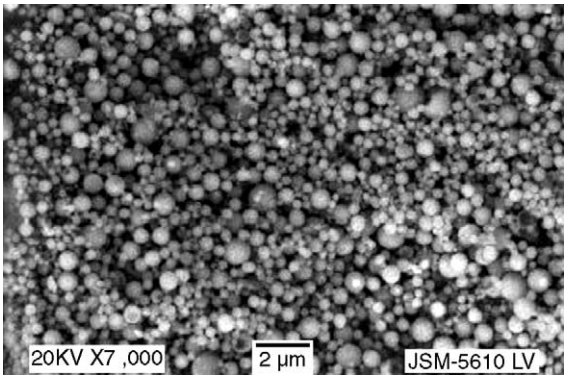

Fig. 1. Scanning electron micrograph of etoposide loaded tripalmitin nanoparticles.

Table 1
Influence of stannous chloride on the labeling efficiency of etoposide and ETPL nanoparticles

a. Influence of amount of stannous chloride on the labeling efficiency of etoposide

$SnCl_2 \cdot 2H_2O$ (μg)	Etoposide		
	% labeled	% colloids	% free
5	80.24	0.45	19.31
10	88.76	0.48	1.76
20	99.28	0.68	0.04
25	98.25	1.18	0.57
50	96.78	3.01	0.21

b. Influence of amount of stannous chloride on the labeling efficiency of ETPL nanoparticles

$SnCl_2 \cdot 2H_2O$ (μg)	ETPL		
	% labeled	% colloids	% free
10	85.74	0.25	14.01
30	92.26	0.38	7.36
60	98.85	0.68	0.47
75	94.48	3.85	1.67
100	92.85	7.01	0.14

Each value is the mean of three experiments.
ETPL—Etoposide loaded tripalmitin nanoparticles.

Etoposide and ETPL nanoparticles were radiolabeled with ^{99m}Tc with high labeling efficiency. The pertechnetate which exists in heptavalent oxidation state was reduced to lower valence state by stannous chloride and the pH was adjusted to 6.5 before addition of etoposide or ETPL nanoparticle dispersion. The amount of stannous chloride used for reducing the pertechnetate played an important role in the labeling process. The influence of stannous chloride on labeling efficiency and formation of radio colloids is shown in Table 1. The optimum amount of stannous chloride resulting in high labeling efficiency and low amount of radiocolloids was found to be 20 μg for etoposide and 60 μg for ETPL nanoparticles. Lower amounts of stannous chloride led to poor labeling efficiency while higher amounts led to the formation of undesirable radiocolloids. The labeling efficiency and stability of labeled complex were ascertained by ascending thin layer chromatography.

Table 2
In vitro stability of ^{99m}Tc-etoposide and ^{99m}Tc-ETPL nanoparticles in presence of chelating agents

% Transchelation		
Conc (mM)	ET	ETPL
DTPA		
10	1.92 ± 0.16	1.82 ± 0.18
30	3.28 ± 0.19	2.85 ± 0.21
50	4.21 ± 0.25	3.75 ± 0.27
Cysteine		
10	1.65 ± 0.15	1.54 ± 0.17
30	2.68 ± 0.18	2.45 ± 0.14
50	4.52 ± 0.21	4.12 ± 0.24

Each value is the mean (± S.D.) of three experiments. ET—Etoposide, ETPL—Etoposide loaded tripalmitin nanoparticles.

3.1. In vitro stability of labeled complexes

DTPA and cysteine challenge studies were performed to get the information on the transchelation (a measure of strength of binding). Challenge studies demonstrated that the labeling efficiency of the complexes did not alter much in presence of DTPA and cysteine (Table 2). Even at 50 mM concentration of DTPA and cysteine, the transchelation was found to be less than 5% for etoposide and ETPL nanoparticles indicating the in vitro stability of the radiolabeled complexes.

Table 3 represents the data of in vitro serum stability of ^{99m}Tc labeled complexes of etoposide and ETPL nanoparticles determined up to 24 h. The data demonstrated stability of the labeled complexes in serum up to 24 h as indicated by their labeling efficiency (97.79% and 97.12% labeling efficiency at 24 h for etoposide and ETPL nanoparticles, respectively). The serum stability of the labeled complexes indicates their usefulness as markers for the biodistribution studies.

3.2. Biodistribution study

The biodistribution studies of ^{99m}Tc-etoposide and ^{99m}Tc-ETPL nanoparticles were performed after intravenous (injection into the tail vein), intraperitoneal or subcutaneous injection in mice at 1 h, 6 h and 24 h post-injection. After intravenous injection, greater concentrations of etoposide were found in heart, kidney, muscle, bone and the organs of RES such as liver, spleen and lung (Table 4) compared to that of i.p. and s.c. route. The over all distribution of ETPL nanoparticles to liver, lung and spleen was significantly lower than the free etoposide ($P<0.001$). However, significant quantity of ETPL nanoparticles was found in liver (1.58% ID) and lung (5.51% ID) at 1 h post-injection. The splenic uptake of ETPL nanoparticles was low initially (0.15% ID at 1 h), but increased with time (0.85% and 1.78% ID at 6 h and 24 h post-injection, respectively). The uptake of free etoposide by lung tissues was high initially (9.91% ID at 1 h post-injection) followed by a decrease later (6.47% and 2.99% ID at 4 h and 24 h post-injection, respectively). A reverse trend was observed for nanoparticles where the uptake by lung increased with time (5.51% and 6.88% ID at 1 h and 6 h, respectively). The lower concentration of ETPL nanoparticles in kidneys all the time compared to etoposide ($P<0.001$) indicates their slower excretion. ETPL nanoparticles exhibited significantly lower cardiac concentrations compared to free etoposide. The distribution of ETPL nanoparticles to muscle and bone increased with time. However, the bone concentrations of ETPL nanoparticles were significantly lower ($P<0.001$) than the free etoposide at all the time points studied. A very low overall radioactivity recovered from the stomach and intestine indicates the in vivo stability of the ^{99m}Tc labeled complexes. The tumor uptake of both etoposide and ETPL nanoparticles after intravenous injection was very low initially (0.015% and 0.025% ID respectively at

Table 3
Stability of ^{99m}Tc labeled etoposide and ETPL nanoparticles in human serum

% Radiolabeling		
Time (h)	ET	ETPL
Initial	99.28	98.85
0.25	99.20	98.80
0.5	99.22	98.78
1	99.10	98.68
2	99.01	98.31
4	98.94	98.12
8	98.78	98.02
24	97.79	97.12

Each value is the mean of three experiments. ET—Etoposide, ETPL—Etoposide loaded tripalmitin nanoparticles.

Table 4
Biodistribution of ^{99m}Tc-etoposide and ^{99m}Tc-ETPL nanoparticles after intravenous injection in Balb/c mice bearing Dalton's lymphoma tumor

Percent injected dose per gm of organ/tissue (± S.E.M.)						
Organ/tissue	1 h		6 h		24 h	
	ET	ETPL	ET	ETPL	ET	ETPL
Blood	0.78 ± 0.01	0.38 ± 0.01[a]	0.48 ± 0.02	0.32 ± 0.02[a]	0.18 ± 0.01	0.15 ± 0.01
Heart	0.16 ± 0.01	0.03 ± 0.01[a]	0.12 ± 0.01	0.03 ± 0.01[a]	0.11 ± 0.01	0.01 ± 0.02[a]
Liver	4.10 ± 0.06	1.58 ± 0.05[a]	3.49 ± 0.04	1.41 ± 0.06[a]	3.12 ± 0.04	2.21 ± 0.04[a]
Lung	9.91 ± 0.17	5.51 ± 0.12[a]	6.47 ± 0.07	6.88 ± 0.10	2.99 ± 0.04	1.00 ± 0.09[a]
Spleen	11.05 ± 0.13	0.15 ± 0.03[a]	9.84 ± 0.13	0.85 ± 0.02[a]	8.83 ± 0.11	1.78 ± 0.03[a]
Kidney	2.75 ± 0.06	0.34 ± 0.15[a]	1.26 ± 0.05	1.19 ± 0.09[a]	1.6 ± 0.05	0.42 ± 0.05[a]
Muscle	0.06 ± 0.02	0.01 ± 0.01[b]	0.03 ± 0.01	0.02 ± 0.01	0.08 ± 0.02	0.05 ± 0.01
Bone	0.14 ± 0.03	0.05 ± 0.02[a]	0.24 ± 0.02	0.12 ± 0.02[a]	0.68 ± 0.03	0.41 ± 0.08[a]
Stomach	0.23 ± 0.06	1.16 ± 0.03	0.35 ± 0.03	1.38 ± 0.01[a]	0.37 ± 0.04	0.34 ± 0.03
Intestine	0.54 ± 0.08	0.15 ± 0.03	0.37 ± 0.04	0.42 ± 0.04	0.09 ± 0.05	0.12 ± 0.01
Brain	0.01 ± 0.01	0.01 ± 0.01	0.01 ± 0.01	0.01 ± 0.01	0.01 ± 0.01	0.02 ± 0.04

The animals were intravenously administered with 100 μCi of the ^{99m}Tc-etoposide and ^{99m}Tc-ETPL nanoparticles and were sacrificed at 1 h, 6 h and 24 h post-injection. Radioactivity was counted in each organ and expressed as percent injected dose per gm of organ/tissue. Each value is the mean (± SEM) of 3 mice.
ET indicates Etoposide, ETPL indicates Etoposide loaded tripalmitin nanoparticles.
[a] Indicates extremely significant ($P<0.001$).
[b] Indicates very significant($P<0.01$).

1 h post-injection) followed by a slight increase with time (0.04% and 0.052% ID respectively at 24 h post-injection) (Fig. 2). The over all tumor concentration of ETPL nanoparticles was significantly higher than free etoposide ($P<0.001$).

After intraperitoneal injection, the distribution of ETPL nanoparticles to all the tissues was significantly higher than etoposide ($P<0.001$) at 1 h post-injection indicating their rapid disposition from peritoneum (Table 5). The concentration of etoposide in all the organs studied increased at 6 h post-injection. The distribution of ETPL nanoparticles to liver and lung increased, but the distribution to spleen, muscle and bone decreased at 6 h post-injection. A progressive increase in concentration of both etoposide and ETPL nanoparticles in blood was observed with time. The uptake of ETPL nanoparticles by liver and lung decreased, while that of spleen increased significantly at 24 h post-injection. The ETPL nanoparticles also showed a significantly higher muscle and bone concentrations than free etoposide. The overall brain distribution of ETPL nanoparticles was significantly higher than free etoposide. Importantly, the uptake of nanoparticles by stomach and intestine was significantly higher than the free etoposide (500 folds in stomach and 56 folds in intestine) ($P<0.001$). The tumor uptake of both etoposide and ETPL nanoparticles increased with time. The overall tumor uptake of ETPL nanoparticles was significantly higher than free etoposide ($P<0.001$) (Fig. 3). In comparison, the overall tumor concentrations of both etoposide and ETPL nanoparticles were significantly higher than after intravenous administration ($P<0.001$).

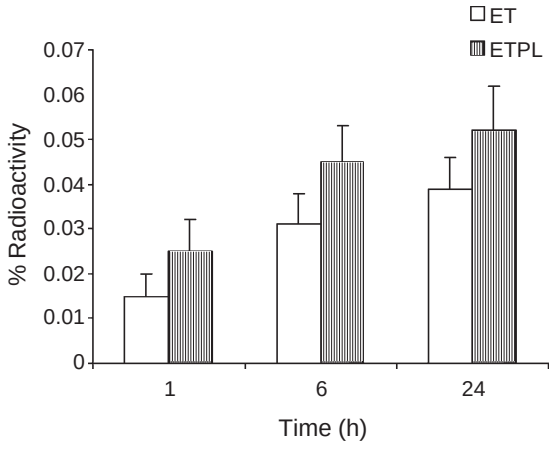

Fig. 2. Tumor concentrations of ^{99m}Tc-etoposide and ^{99m}Tc-ETPL nanoparticles after intravenous injection in Dalton's lymphoma tumor bearing mice. Each value is the mean (± S.D.) of three experiments. ET—Etoposide, ETPL—Etoposide loaded tripalmitin nanoparticles.

Table 5
Biodistribution of ^{99m}Tc-etoposide and ^{99m}Tc-ETPL nanoparticles after intraperitoneal injection in Balb/c mice bearing Dalton's lymphoma tumor

Percent injected dose per gm of organ/tissue (± S.E.M.)						
Organ/tissue	1 h		6 h		24 h	
	ET	ETPL	ET	ETPL	ET	ETPL
Blood	0.04 ± 0.01	0.33 ± 0.02[a]	0.22 ± 0.03	0.38 ± 0.02[a]	0.23 ± 0.03	0.40 ± 0.03[a]
Heart	0.02 ± 0.01	0.13 ± 0.01[a]	0.14 ± 0.02	0.10 ± 0.03[b]	0.37 ± 0.03	0.35 ± 0.02
Liver	0.05 ± 0.01	0.83 ± 0.04[a]	0.83 ± 0.04	1.50 ± 0.06[a]	0.22 ± 0.04	0.82 ± 0.06[a]
Lung	0.033 ± 0.01	0.36 ± 0.03[a]	0.18 ± 0.02	0.74 ± 0.07[a]	0.36 ± 0.04	0.36 ± 0.06
Spleen	0.014 ± 0.01	2.75 ± 0.12[a]	0.60 ± 0.02	2.16 ± 0.21[a]	0.32 ± 0.05	3.07 ± 0.21[a]
Kidney	0.16 ± 0.01	3.62 ± 0.14[a]	1.00 ± 0.05	3.41 ± 0.18[a]	0.53 ± 0.05	1.87 ± 0.05[a]
Muscle	0.01 ± 0.01	0.45 ± 0.03[a]	0.35 ± 0.01	0.08 ± 0.01[a]	0.05 ± 0.02	0.30 ± 0.06[a]
Bone	0.02 ± 0.01	0.29 ± 0.02[a]	0.19 ± 0.02	0.18 ± 0.02	0.09 ± 0.03	0.54 ± 0.07[a]
Stomach	0.014 ± 0.01	7.0 ± 0.31[a]	0.30 ± 0.03	1.03 ± 0.04[a]	0.17 ± 0.04	2.24 ± 0.15[a]
Intestine	0.03 ± 0.02	1.70 ± 0.12[a]	0.36 ± 0.03	1.52 ± 0.08[a]	0.06 ± 0.02	1.79 ± 0.12[a]
Brain	0.003 ± 0.01	0.11 ± 0.02[a]	0.02 ± 0.01	0.013 ± 0.01	0.06 ± 0.01	0.13 ± 0.04[a]

The animals were intraperitoneally administered with 100 μCi of the ^{99m}Tc-etoposide and ^{99m}Tc-ETPL nanoparticles and were sacrificed at 1 h, 6 h and 24 h post-injection. Radioactivity was counted in each organ and expressed as percent injected dose per gm of organ/tissue. Each value is the mean (± S.E.M.) of 3 mice.
ET indicates Etoposide, ETPL indicates Etoposide loaded tripalmitin nanoparticles.
[a] Indicates extremely significant ($P < 0.001$).
[b] Indicates very significant ($P < 0.01$).

After subcutaneous injection, etoposide showed rapid distribution to blood, heart, liver, lung and kidney (Table 6). The higher concentration of etoposide in kidney compared to ETPL nanoparticles at 1 h post-injection suggests its rapid clearance from site of injection. The concentration of nanoparticles increased in liver, spleen and kidney at 6 h and 24 h post-injection indicating its disposition with time from the injection site. The concentration of etoposide in liver, lung and kidney decreased, and a slight increase in spleen and muscle was observed at 24 h post-injection. The concentration of nanoparticles experienced a significant increase in heart, liver, spleen, kidney and bone at 24 h post-injection. The uptake of etoposide by bone increased with time. The overall uptake of ETPL nanoparticles by bone was significantly higher than free etoposide. The tumor uptake of etoposide and ETPL nanoparticles was low initially followed by a significant increase with time. The ETPL nanoparticles experienced significantly higher tumor uptake than free etoposide at all time points of the study (Fig. 4).

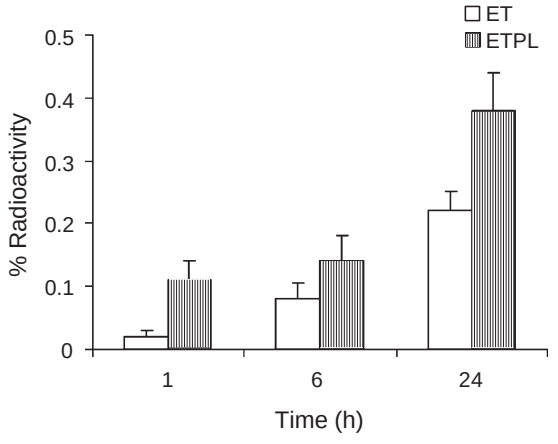

Fig. 3. Tumor concentrations of ^{99m}Tc-etoposide and ^{99m}Tc-ETPL nanoparticles after intraperitoneal injection in Dalton's lymphoma tumor bearing mice. Each value is the mean (± S.D.) of three experiments. ET—Etoposide, ETPL—Etoposide loaded tripalmitin nanoparticles.

Comparatively, the subcutaneous injection resulted in a significant reduction in the uptake of ETPL nanoparticles by organs of RES such as liver, lung and spleen. The distribution of nanoparticles to liver and lung was of the order of subcutaneous < intraperitoneal < intravenous route. The overall kidney concentration of ETPL nanoparticles was comparatively low after subcutaneous injection indicating slower excretion. The cardiac concentrations of ETPL nanoparticles were low after subcutaneous injection. Of the three different routes of injection studied, the intra-

Table 6
Biodistribution of ^{99m}Tc-etoposide and ^{99m}Tc-ETPL nanoparticles after subcutaneous injection in Balb/c mice bearing Dalton's lymphoma tumor

Percent injected dose per gm of organ/tissue (± S.E.M.)						
Organ/tissue	1 h		6 h		24 h	
	ET	ETPL	ET	ETPL	ET	ETPL
Blood	0.32 ± 0.04	0.22 ± 0.04[a]	0.19 ± 0.03	0.17 ± 0.04	0.08 ± 0.01	0.19 ± 0.03[a]
Heart	0.14 ± 0.02	0.09 ± 0.01[a]	0.08 ± 0.02	0.07 ± 0.03	0.08 ± 0.02	0.13 ± 0.02[a]
Liver	0.30 ± 0.03	0.09 ± 0.01[a]	0.21 ± 0.04	0.18 ± 0.03	0.28 ± 0.06	0.47 ± 0.06[a]
Lung	0.18 ± 0.02	0.14 ± 0.04	0.14 ± 0.02	0.12 ± 0.03	0.08 ± 0.02	0.14 ± 0.04[a]
Spleen	0.05 ± 0.01	0.06 ± 0.02	0.04 ± 0.02	0.10 ± 0.02	0.07 ± 0.03	0.16 ± 0.03[a]
Kidney	1.40 ± 0.10	0.70 ± 0.04[a]	0.91 ± 0.08	1.10 ± 0.12	0.68 ± 0.04	1.82 ± 0.13[a]
Muscle	0.05 ± 0.01	0.04 ± 0.03	0.02 ± 0.01	0.03 ± 0.01	0.04 ± 0.01	0.05 ± 0.02
Bone	0.09 ± 0.01	0.16 ± 0.04[a]	0.10 ± 0.02	0.12 ± 0.02	0.18 ± 0.03	0.22 ± 0.05[b]
Stomach	0.28 ± 0.04	0.38 ± 0.08	0.25 ± 0.05	0.23 ± 0.05	0.16 ± 0.04	0.94 ± 0.05[a]
Intestine	0.24 ± 0.05	0.05 ± 0.01	0.38 ± 0.06	0.32 ± 0.07	0.59 ± 0.04	1.31 ± 0.10[a]
Brain	0.02 ± 0.01	0.01 ± 0.01	0.01 ± 0.01	0.01 ± 0.01	0.02 ± 0.01	0.03 ± 0.01

The animals were subcutaneously administered with 100 μCi of the ^{99m}Tc-etoposide and ^{99m}Tc-ETPL nanoparticles and were sacrificed at 1 h, 6 h and 24 h post-injection. Radioactivity was counted in each organ and expressed as percent injected dose per gm of organ/tissue. Each value is the mean (± S.E.M.) of 3 mice.

ET indicates Etoposide, ETPL indicates Etoposide loaded tripalmitin nanoparticles.

[a] Indicates extremely significant ($P < 0.001$).

[b] Indicates very significant ($P < 0.01$).

peritoneal injection of ETPL nanoparticles resulted in significantly higher brain distribution. Etoposide and ETPL nanoparticles administered by subcutaneous injection experienced a significantly higher tumor uptake, and after any route of injection studied, the ETPL nanoparticles showed greater tumor concentrations than free etoposide.

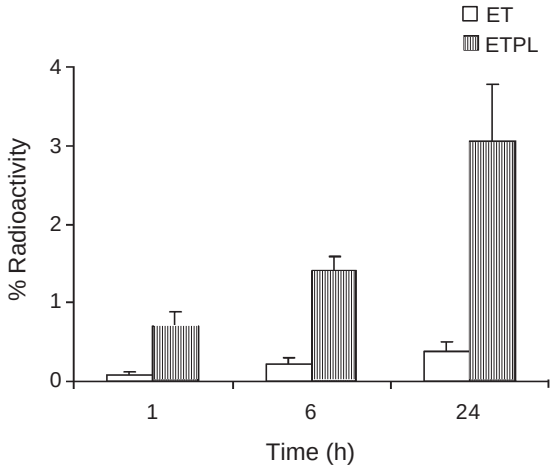

Fig. 4. Tumor concentrations of ^{99m}Tc-etoposide and ^{99m}Tc-ETPL nanoparticles after subcutaneous injection in Dalton's lymphoma tumor bearing mice. Each value is the mean (± SD) of three experiments. ET—Etoposide, ETPL—Etoposide loaded tripalmitin nanoparticles.

4. Discussion

The main objective of the present study is to evaluate the biodistribution and tumor uptake of etoposide and ETPL nanoparticles after three different routes such as intravenous, intraperitoneal and subcutaneous injection and determine the superior administration route offering high tumor uptake and retention of nanoparticles. The melt-emulsification and high pressure homogenization technique followed by spray drying offered spherical nanoparticles with 387 nm mean diameter. The nanoparticles obtained by this technique were stable with a mean particle diameter of 389 nm even after 4 months of preparation. The nanoparticles also offered excellent resdispersibility and did not require any sort of energy such as ultrasonication at the time of dispersion.

Studies with different amounts of stannous chloride were carried out to optimize parameters for maximum radiolabeling efficiency. The amount of stannous chloride above the optimum concentration results in undesirable colloid formation, and these radiocolloids

distribute extensively to the organs of reticuloendothelial system due to their macrophage uptake. The stannous chloride below the optimum concentration leads to poor labeling efficiency due to the incomplete reduction of pertechnetate (TcO_4^-) from its heptavalent oxidation state. Hence, optimization of the amount of stannous chloride is an important parameter in the radiolabeling of a compound. The in vitro stability of nanoparticles was assessed by DTPA and cysteine challenge test. DTPA and cysteine possess greater affinity to ^{99m}Tc. Upon incubation with the labeled complexes, the DTPA and cysteine causes transchelation resulting in decrease in labeling of the complexes. The degree of transchelation was low for both ^{99m}Tc-etoposide and ^{99m}Tc-ETPL nanoparticle complex indicating their high degree of in vitro stability. Etoposide possess three binding sites of hydroxyl (−OH) groups at position 4 (4-hydroxy-3,5-dimethoxyphenyl residue) and in the glucopyranosyl moiety, which can participate in coordination. Possibly, two molecules of Etoposide bind with Tc-99 m to form stable complexes.

After challenging with DTPA, the labeled compound does not dissociate because DTPA provides the hard donor atoms while ^{99m}Tc is a soft Lewis acid, since DTPA and etoposide technetium-99 m complexes are co-ordinated through O-donor atoms, which do not allow dissociation.

If we compare stability constants under chemical environment (not under physiological conditions), the stability of the former will be much higher than that of etoposide complex. However, we did not observe significant transchelation, which could be explained by utilization of two molecules of etoposide as proposed above (Fig. 5).

Determination of stability of the labeled complexes in serum is an important parameter, which assures the intactness of the label in presence of proteins and many other substances present in the serum. The stability of labeled complexes in serum also supports their stability in biological environment upon administration into the body and their use in determining the biodistribution patterns.

The uptake and distribution into tissues of both etoposide and ETPL nanoparticles were different after different routes of injection. Incorporation of etoposide into nanoparticles has significantly reduced the initial uptake by organs of RES such as liver, lung and spleen and other organs such as kidney, muscle

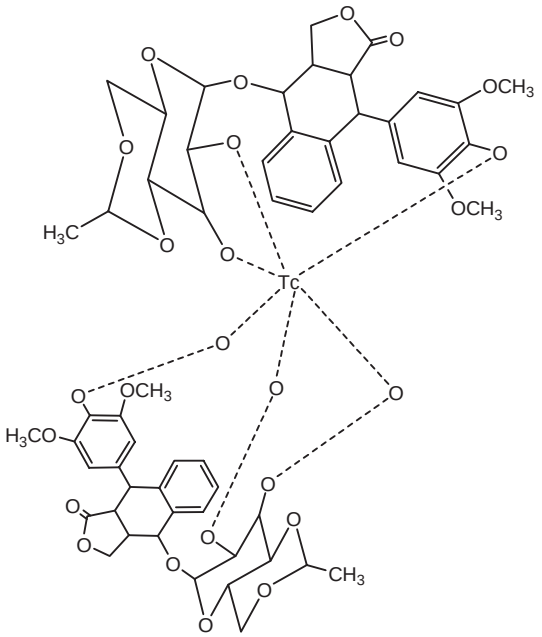

Fig. 5. Radiolabeled complex of ^{99m}Tc-etoposide.

and bone. This shows that the biodistribution of etoposide is greatly controlled by the nanoparticles. After intraperitoneal administration, the ETPL nanoparticles showed a biphasic absorption into blood. An initial rapid distribution of ETPL nanoparticles compared to etoposide to all the tissues studied suggests their rapid absorption into blood. Followed by the initial rapid distribution, the later slow appearance of etoposide and ETPL nanoparticles in blood with time suggests their slow disposition from peritoneum. This is further supported by the increase in liver and lung concentrations of nanoparticles at 6 h post-injection and significantly higher spleen concentrations at 24 h post-injection. The significantly high brain uptake of ETPL nanoparticles indicated their potential use in the treatment of brain malignancies, as etoposide is also used in treatment of brain malignancies such as brain stem gliomas [18,19]. The uptake of ETPL nanoparticles by stomach and intestine after intraperitoneal injection was significantly higher of all the routes investigated. This can be attributed to the direct penetration of ETPL nanoparticles into stomach and intestine from the peritoneal cavity. Even if we consider for the sake of argument that the higher radioactivity in stomach and intestine after intraperitoneal injection may be due to the leached ^{99m}Tc rather than

the ^{9m}Tc-ETPL nanoparticle complex, the same complex did not give such high concentrations in both the organs after other routes of injection. Also the stability of ^{9m}Tc-ETPL nanoparticle complex has been well established by DTPA and cysteine challenge and serum stability. Such high uptake of nanoparticles by stomach suggests their potential use in the treatment of stomach cancer. The biodistribution data after subcutaneous injection show that the distribution of etoposide is rapid from the injection site indicated by its initial high concentrations in tissues compared to ETPL nanoparticles. The increase in concentration of ETPL nanoparticles in tissues at 6 h and 24 h post-injection indicates its residence at the injection site for longer time. The distribution of both etoposide and ETPL nanoparticles to organs of RES such as liver, lung and spleen was in the order of intravenous > intraperitoneal > subcutaneous injection. This is in accordance with that observed by Allen and coworkers [14] in case of liposomes. The high overall uptake of ETPL nanoparticles by bone can be attributed to their ingestion by bone-marrow derived macrophages after subcutaneous injection [14].

The Dalton's lymphoma implanted in the right hind limb of mice is of T-cell lymphoma type [27]. According to Muranishi and coworkers [15] and Takahashi [16], tumor cells that have invaded a lymphatic vessel would be trapped in the meshwork of a lymph node. We feel that in Dalton's lymphoma, it is the regional lymph nodes which are much affected by the injected tumor cells. Hence, it would be also needed to target the regional lymph nodes of the hind leg region for effective tumor therapy. We have evaluated the tumor uptake of both etoposide and ETPL nanoparticles after intravenous, intraperitoneal and subcutaneous routes of injection. The tumor uptake of both etoposide and ETPL nanoparticles was in the order of subcutaneous > intraperitoneal > intravenous injection. The very low tumor distribution after intravenous injection can be attributed to the barriers hindering the transport of drug and particles into solid tumor such as highly disorganized tumor vasculature, high viscosity of blood within the tumors and abnormally high pressure in the interstitial matrix retarding the molecular transport across the vessel walls and into the interstitium [28]. After intraperitoneal injection, the major quantities of drug and ETPL nanoparticles remained in the peritoneum for longer time resulting in poor distribution to tumor. Though it is expected that hydrophobic and negatively charged ETPL nanoparticles penetrate the interstitium adjacent to the peritoneal wall and gain access to the lymph nodes, the intraperitoneal route did not result in significant tumor concentration. The possible explanations may be the formation of depot in peritoneum, high uptake by the organs of the peritoneal cavity and also non-specific distribution from peritoneum due to very high surface area of peritoneal cavity.

The initial lower tumor uptake followed by increase with time after subcutaneous injection suggests slower disposition of etoposide and ETPL nanoparticles from the injection site into the tumor. The significantly high tumor uptake of ETPL nanoparticles indicates their greater penetration through the tumor interstitium. The drug transport into tumors is determined by several factors. As mentioned by Markman [29] and Song [30], the distribution to tumors after intratumoral or intravesical administration (injection in the peritumoral space) is by diffusion through the interstitial space. Earlier studies using tumor cell spheroids showed that the penetration of anticancer agent doxorubicin after intravesical injection is limited to the periphery [31,32]. Such slow drug disposition into tumor may be due to the hindrance to drug penetration in the interstitial space. Kuh and co-workers [33,34] observed differences in accumulation of paclitaxel in monolayers and histocultures of human pharynx FaDu xenograft tumors. The drug accumulation was more and rapid in monolayers and a more rapid attainment of pseudo steady state between extracellular and intracellular drug concentrations (at 4 h) whereas the histocultures showed lower drug accumulation and took longer time (48 h) to reach the pseudo steady state. This indicates that the factors specifically related to 3-dimensional structures determine the rate of drug penetration and extent of drug accumulation and retention in solid tumors. Recent work by Au and co-workers [35] showed that tumors with lower tumor cell fraction and greater interstitial space resulted in rapid tumor penetration indicating the spatial relationship between tumor architecture, tumor cell distribution and drug penetration. Also an abrupt increase in the drug penetration rate was observed in the xenograft tumor after 24 h (drug penetrated 15 cell layers in the periphery in first 24 h but more than 80 cell layers in the next 24 h). Au and coworkers [35] observed that the treatment concentra-

tions also influenced the tumor transport of drugs. This was confirmed with apoptotic inducing drugs such as doxorubicin and paclitaxel, wherein the drug penetration into tumors increased with concentrations required to induce apoptosis, whereas a poor drug transport confined to periphery at the concentrations lower than that required to induce apoptosis. The drug penetration into tumor was well coincided with the apoptosis induction and expansion of interstitial space with the tumor drug penetration. The same has been observed in case of histocultures of human PC3 prostate xenograft tumors. At lower drug concentrations, the drug remained at the periphery while at apoptotic concentrations, the drug was initially confined to the periphery up to 24 h, followed by an abruptly enhanced drug penetration at 36 h. The increased tumor penetration of apoptotic inducers such as doxorubicin and paclitaxel at apoptotic concentrations was attributed to the apoptosis and gradual reduction in cell density in the penetration path of drug and thereby the enhanced tumor penetration [35]. The higher tumor penetration of ETPL nanoparticles in our case can be attributed to their enhanced cell penetration due to smaller size, resulting in effective apoptosis and reduction in tumor cell density from periphery to the center of the tumor. The higher tumor concentration of ETPL nanoparticles at 24 h post-injection is also confirmed by tumor imaging (Fig. 6) and indicated prolonged tumor retention facilitating effective and prolonged tumor therapy. (The gamma image of mice after intraperitoneal injection is not shown because most of the injected radiolabeled complex remained in the peritoneal cavity, and the contrastness of peritoneum was so high that the other part of the body was not visible in the image). From the biodistribution data, we confirm that the distribution of etoposide is greatly controlled when delivered through tripalmitin nanoparticles, and subcutaneous administration of nanoparticles below the tumor region facilitates significant tumor uptake which is expected to result in effective tumor therapy followed by tumor regression.

5. Conclusions

Etoposide loaded tripalmitin nanoparticles prepared by melt emulsification and homogenization, followed by spray drying technique were spherical and possessed negative charge. The physicochemical properties of nanoparticles are well suited with the requirements for penetration through lymphatic interstitium. The relatively low tissue distribution of ETPL nanoparticles after subcutaneous injection is advanta-

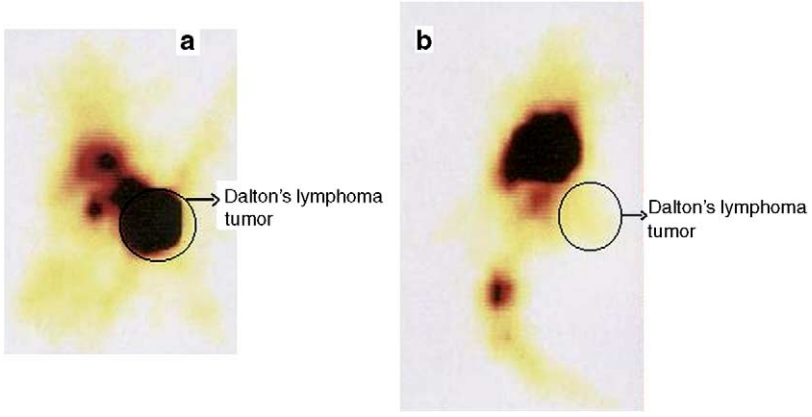

Fig. 6. Gamma scintigraphic images of mice bearing Dalton's lymphoma tumor at 24 h post-injection of ^{99m}Tc-ETPL nanoparticles by subcutaneous or intravenous route. The circle portions in both the figures indicate the Dalton's lymphoma tumor implanted in hind leg of Balb/c mice. Panel (a) represents the gamma image of tumor bearing mice after subcutaneous injection of ^{99m}Tc-ETPL nanoparticles taken at 24 h post-injection demonstrating the significant tumor uptake and retention (the black portion in the figure indicates radiolabeled complex). Panel (b) represents the gamma image of tumor bearing mice after intravenous injection of ^{99m}Tc-ETPL nanoparticles through tail vein, taken at 24 h post-injection demonstrating poor tumor uptake. The tumor uptake and retention after subcutaneous injection is significantly higher (~59 folds) than after intravenous injection.

geous in reducing the etoposide associated systemic toxicity. The higher brain concentration of ETPL nanoparticles after intraperitoneal injection indicates their potential use in targeting etoposide to brain tumors. A significant fold higher uptake of ETPL nanoparticles by stomach after intraperitoneal injection suggests their potential use in therapy of stomach cancer. The accumulation of ETPL nanoparticles at the administration site after subcutaneous injection is advantageous in facilitating prolonged tumor therapy. The significantly higher tumor uptake of ETPL nanoparticles than free etoposide after any route of injection studied indicates the advantage of delivering etoposide through tripalmitin nanoparticles in enhancing the tumor uptake. Finally, the tripalmitin nanoparticles are an efficient delivery system for etoposide in controlling the biodistribution which ultimately results in reducing the systemic toxicity. Subcutaneous injection near the tumor site is the route of preference for facilitating high tumor uptake and retention and is likely to have greater antitumor effect resulting in tumor regression.

Acknowledgements

Financial support from the University Grants Commission (F.10-32/2000 (SA-II)) New Delhi, India is gratefully acknowledged. Maj. Gen. T. Ravindranath, AVSM, VSM, Director, Institute of Nuclear Medicine and Allied Sciences, Delhi, India is acknowledged for providing necessary facilities to carry out the radiolabeling and biodistribution studies. LHVR and RSRM are grateful to Mr. M.N. Patel, Department of Metallurgy, M.S. University of Baroda, India for his help in obtaining scanning electron micrograph.

References

[1] T. Nomura, A. Saikawa, S. Morita, T. Sakaeda, F. Yamashita, K. Honda y. Takakura, M. Hahida, Pharmacokinetic characteristics and therapeutic effects of mitomycin C-dextran conjugates after intratumoral injection, J. Control. Release 52 (1998) 239–252.

[2] H. Seong, T.K. An, G. Khang, S.-U. Choi, C.O. Lee, H.B. Lee, BCNU-loaded poly (D,L-lactide-co-glycolide) wafer and antitumor activity against XF-498 human CNS tumor cells in vitro, Int. J. Pharm. 251 (2003) 1–12.

[3] H. Maeda, T. Sawa, T. Konno, Mechanism of tumor-targeted delivery of macromolecular drugs, including the EPR effect in solid tumor and clinical overview of prototype polymeric drug SMANCS*, J. Control. Release 74 (2001) 47–61.

[4] T. Nakanishi, S. Fukushima, K. Okamoto, M. Suzuki, Y. Matsumura, M. Yokoyama, T. Okano, Y. Sakurai, K. Kataoka, Development of the polymer micelle carrier system for doxorubicin, J. Control. Release 74 (2001) 295–302.

[5] W. Junping, K. Takayama, T. Nagai, Y. Maitani, Pharmacokinetics and antitumor effects of vincristine carried by microemulsions composed of PEG-lipid, oleic acid vitamin E and cholesterol, Int. J. Pharm. 251 (2003) 13–21.

[6] A. Marin, H. Sun, G.A. Husseini, W.G. Pitt, D.A. Christensen, N.Y. Rapoport, Drug delivery in pluronic micelles: effect of high-frequency ultrasound on drug release from micelles and intracellular uptake, J. Control. Release 84 (2002) 39–47.

[7] J.S. Chawla, M.M. Amiji, Biodegradable poly(ε-caprolactone) nanoparticles for tumor-targeted delivery of tamoxifen, Int. J. Pharm. 249 (2002) 127–138.

[8] C. Vauthier, C. Dubernet, C. Chauvierre, I. Brigger, P. Couvreur, Drug delivery to resistant tumors: the potential of poly(alkyl cyanoacrylate) nanoparticles, J. Control. Release 93 (2003) 151–160.

[9] J. Williams, R. Lansdown, R. Sweitzer, M. Romanowski, R. LaBell, R. Ramaswami, E. Unger, Nanoparticle drug delivery system for intravenous delivery of topoisomerase inhibitors, J. Control. Release 91 (2003) 167–172.

[10] R.H. Muller, W. Mehnert, J.S. Lucks, C. Schwarz, A. zur Muhlen, H. Weyhers, C. Freitas, D. Ruhl, Solid lipid nanoparticles (SLN)—an alternative colloidal drug carrier system for controlled drug delivery, Eur. J. Pharm. Biopharm. 41 (1995) 62–69.

[11] C. Schwarz, W. Mehnert, J.S. Lucks, R.H. Muller, Solid lipid nanoparticles (SLN) for controlled drug delivery: I. Production, characterization and sterilization, J. Control. Release 30 (1994) 83–96.

[12] R.H. Muller, H. Maassen, C. Schwarz, W. Mehnert, Solid lipid nanoparticles (SLN) as potential carrier for human use: interaction with human granulocytes, J. Control. Release 47 (1997) 261–269.

[13] R.H. Muller, H. Maassen, H. Weyhers, W. Mehnert, Phagocytic uptake and cytotoxicity of solid lipid nanoparticles (SLN) sterically stabilized with Poloxamine 908 and Poloxamer 407, J. Drug Target. 4 (1996) 161–170.

[14] T.M. Allen, C.B. Hansen, L.S.S. Guo, Subcutaneous administration of liposomes: a comparison with the intravenous and intraperitoneal routes of injection, Biochim. Biophys. Acta 1150 (1993) 9–16.

[15] S. Muranishi, T. Fujita, M. Murakami, A. Yamamoto, Potential for lymphatic targeting of peptides, J. Control. Release 46 (1997) 157–164.

[16] T. Takahashi, Emulsion and activated carbon in chemotherapy CRC, Crit. Rev. Ther. Drug Carr. Syst. 2 (1985) 245–274.

[17] C.J.H. Porter, Drug delivery to the lymphatic system, Crit. Rev. Ther. Drug Carr. Syst. 14 (1997) 333–393.

[18] M. Chamberlain, Recurrent brainstem gliomas treated with oral VP-16, J. Neuro-Oncol. 15 (1993) 133–139.

[19] D. Ashley, L. Meier, T. Kerby, F. Zlduondo, H. Friedman, A. Gajjar, L. Kun, P. Duffner, S. Smith, D. Longee, Response of recurrent medulloblastoma to low-dose oral etoposide, J. Clin. Oncol. 14 (1996) 1922–1927.
[20] C. Oussoren, M. Velinova, G. Scherphof, J.J. van der Want, N. van Rooijen, G. Storm, Lymphatic uptake and biodistribution of liposomes after subcutaneous injection: IV. Fate of liposomes in regional lymph nodes, Biochim. Biophys. Acta 1370 (1998) 259–272.
[21] K. Hirano, C.A. Hunt, Lymphatic transport of liposome encapsulated agents: effect of liposome size following intraperitoneal administration, J. Pharm. Sci. 9 (1985) 915–922.
[22] S.M. Moghimi, A.C. Hunter, J.C. Murray, Long-circulating and target-specific nanoparticles: theory to practice, Pharmacol. Rev. 53 (2001) 283–318.
[23] N. Arulsudar, N. Subramanian, P. Mishra, R.K. Sharma, R.S.R. Murthy, Preparation, characterization and biodistribution of ^{99m}Tc-labeled liposome encapsulated cyclosporine, J. Drug Target. 11 (2003) 187–196.
[24] V.J. Richardson, K. Jeyasingh, R.F. Jewkes, Properties of [^{99m}Tc] technetium labeled liposomes in normal and tumor bearing rats, Biochem. Soc. Trans. 5 (1977) 290–291.
[25] A.E. Theobald, in: C.B. Sampson (Ed.), Text Book of Radiopharmacy: Theory and Practice, Gordon and Breach, New York, 1990, pp. 127–129.
[26] A.K. Mishra, N. Iznaga-Escobar, R. Figueredo, V.K. Jain, B.S. Dwarakanath, R. Perez-Rodriguez, R.K. Sharma, T. Lazar Mathew, Preparation and comparative evaluation of ^{99m}Tc-labeled 2-Iminothiolane modified antibodies and CITC-DTPA immunoconjugates of anti-EGF-receptor antibodies, Methods Find. Exp. Clin. Pharmacol. 24 (2002) 653–660.
[27] P. Shrivastava, S.M. Singh, N. Singh, Effect of thymosin-alpha1 on the production of nitric oxide by tumor-associated macrophages, Neoplasma 50 (2003) 47–50.
[28] R.K. Jain, Barriers to drug delivery in solid tumors, Sci. Am. 271 (1994) 58–65.
[29] M. Markman, Intraperitoneal therapy of ovarian cancer, Semin. Oncol. 25 (1998) 356–360.
[30] D. Song, M.G. Wientjes, J.L.S. Au, Bladder tissue pharmacokinetics of intravesical taxol, Cancer Chemother. Pharmacol. 40 (1997) 285–292.
[31] R.E. Durand, Distribution and activity of antineoplastic drugs in a tumor model, J. Natl. Cancer Inst. 81 (1989) 146–152.
[32] R.E. Durand, Slow penetration of anthracyclines into spheroids and tumors: a therapeutic advantage, Cancer Chemother. Pharmacol. 26 (1990) 198–204.
[33] H.J. Kuh, S.H. Jang, M.G. Wientjes, J.R. Weaver, J.L. Au, Determinants of paclitaxel penetration and accumulation in human solid tumor, J. Pharmacol. Exp. Ther. 290 (1999) 871–880.
[34] H.J. Kuh, S.H. Jang, M.G. Wientjes, J.L. Au, Computational model of intracellular pharmacokinetics of paclitaxel, J. Pharmacol. Exp. Ther. 293 (2000) 761–770.
[35] J.L.-S. Au, S.H. Jang, J. Zheng, C.-T. Chen, S. Song, L. Hu, M.G. Wientjes, Determinants of drug delivery and transport to solid tumors, J. Control. Release 74 (2001) 31–46.